

Article

Inter-Annual Variability of the Seawater Light Absorption in Surface Layer of the Northeastern Black Sea in Connection with Hydrometeorological Factors

Anna Yushmanova ^{1,2}, Oleg Kopelevich ^{1,*}, Svetlana Vazyulya ¹  and Inna Sahling ¹

¹ P. P. Shirshov Institute of Oceanology of the Russian Academy of Sciences (SIO RAS), 117997 Moscow, Russia; yushmanova@phystech.edu (A.Y.); svershova@mail.ru (S.V.); sahling.iv@ocean.ru (I.S.)

² Department of Aerophysics and Space Research, Moscow Institute of Physics and Technology, 141700 Dolgoprudny, Russia

* Correspondence: oleg@ocean.ru; Tel.: +7-916-640-7835

Received: 1 July 2019; Accepted: 16 September 2019; Published: 19 September 2019



Abstract: Data on the light absorption by seawater and its components are needed in many theoretical and practical aspects of marine science and engineering. However, up to now, there is a lack of such data for the northeastern part of the Black Sea. This article presents the data on light absorption measured by a portable integrated cavity absorption meter (ICAM) spectrophotometer in the Gelendzhik region of the Black Sea during field studies in June 2017 and 2018, together with other bio-optical and oceanographic data from in situ measurements and satellite observations. In 2018, the elevated values of the colored dissolved organic matter (CDOM) absorption in the surface layer were observed concurrently with high values of salinity, contradicting the idea of river runoff being the main CDOM source. The vertical profiles of salinity differed in 2017 and 2018, especially in shallow waters; in the upper layer, the salinity increased from 17.1 psu in 2017 to 17.8 psu in 2018, while the values of CDOM absorption increased from 0.10 to 0.16 m⁻¹. The analysis of available hydrometeorological data pointed to intensive vertical mixing due to the strong wind forcing as a main factor in increasing values of both salinity and the CDOM absorption in the surface layer in 2018.

Keywords: seawater light absorption; Black Sea; inter-annual variability; hydrometeorological factors

1. Introduction

This work is aimed at studying the inter-annual variability of the light absorption properties of seawater in the surface layer of the northeastern part of the Black Sea. Absorption, along with scattering, is a basic process governing the light radiation propagation in water from both natural and artificial sources; the absorption parameters are included (directly or indirectly) in the radiation transfer equation and most approximations. Knowledge of the absorption coefficients is needed to assess both spectral transmission and reflectance of a given water layer or the whole water column.

The seawater absorption properties depend on the content of optically active components of seawater, such as the colored dissolved organic matter (CDOM), phytoplankton pigments, detritus and other particles, and the seawater itself. The content of these components varies depending on water types, as well as seasonally and inter-annually. The spectral values of seawater absorption coefficient are very sensitive to variability of these components and reflect their changes. Specialists in different fields need such data in their studies: marine biologists for assessment of the photosynthetically available radiation (PAR) at different depths and assimilation of solar radiation for primary production; physical oceanographers for estimating ocean albedo and volume absorption in water column; marine ecologists for tracking river runoff and propagation of various impurities.

However, despite the theoretical and practical need of absorption data, until recently, the hydro-optical expeditionary research did not practically include direct measurements of spectral seawater light absorption. This was due to the difficulties of measuring true absorption in a weakly absorbing scattering medium such as seawater. Conventional spectrophotometers in scattering media measure the losses of the light beam not only due to the absorption, but also due to scattering. Reliable results also cannot be obtained by calculating the absorption coefficient as the difference between the attenuation and scattering coefficients, since their accuracy is not high enough, and the error of the difference can be significant. Indirect methods, based on the light field theory by using both natural and artificial sources (including lidars and satellite sensors), have their own difficulties; furthermore, these methods limit the possibility of studying individual factors causing the light absorption by seawater.

The problem was practically solved with the idea of using the integrating sphere to collect the scattered light at the photodetector such that the losses were caused only by absorption. This idea was implemented in a laboratory seawater light absorption meter “Volna” [1], which provided the first mass data on spectral light absorption by seawater and its components from measurements in the Atlantic and Pacific Oceans in 1971, as well as in the Baltic Sea [2]. The obtained data showed, in particular, the dominant contribution from CDOM in the shortwave part of the visible spectrum in most cases [3]; the spectral dependency of the CDOM absorption was carefully studied [4].

In the present work, focus is placed on the CDOM absorption. The first studies of CDOM in seawater were carried out by the German chemical oceanographer Kalle who named it “yellow substance”—“gelbstoff” in German [5]. This is the other conventional term for CDOM, and the symbol a_g is used for the CDOM (yellow substance) absorption coefficient.

Active studies of spectral absorption by the yellow substance began in the 1980s [6–9]. In the Black Sea, the first studies of spectral absorption were associated with phytoplankton and focused on the problems of utilization of solar radiation during photosynthesis [9–11]. First measurements of spectral absorption by seawater components, including CDOM, at a modern level, were carried out at the beginning of this century; recently, they were aimed at developing satellite algorithms for the separate determination of absorption by chlorophyll and yellow substance [12,13].

The northeastern part of the Black Sea is a region where intensive coccolithophore blooms (CB) are regularly observed, usually in June [14–17]. Coccolithophore (coccolithophorids) is a single-celled alga with spherical cells surrounded by disc-shaped plates (coccolites) consisting of calcium carbonate, CaCO_3 . Plated cells and detached coccoliths produce a strong nonselective light scattering, which makes it possible to detect CB using a satellite color scanner. CB is a climatically significant factor affecting physical and biogeochemical processes, particularly the exchange of CO_2 between the ocean and atmosphere and global climate change [18]. Owing to strong scattering, CB influences the ocean albedo and, as a result, the heat budget.

Since 2004, regular sea expeditions were carried out in the northeastern Black Sea every June, using the research capabilities of the Southern Branch of the Shirshov Institute of Oceanology Russian Academy of Science (SIO RAS) located near Gelendzhik. Primarily, the work was aimed at studying the coccolithophore blooms. Based on the data of in situ measurements, a regional algorithm for estimating the concentration of coccolithophore cells was developed [14]. The algorithm derives from satellite data the particle backscattering coefficient b_{bp} and takes into account the contribution from “non-coccolithophore” particles brought by river runoff. For that, the yellow substance absorption coefficient a_g is used, which is also calculated from satellite data [14]. The results of these studies are presented in References [15–17].

Satellite observations focused on the eastern open part and the eastern and southern shelves, which correspond to sub-regions #7 and #8 (see Figure 1) according to the demarcation below [19,20].

The analysis of the obtained data confirmed the assumption that it is possible to use a_g for estimating the contribution of particles brought by river runoff to the particle backscattering coefficient b_{bp} and for estimating the terrigenous component TSM_trg of the suspended matter. According to data from 2005–2007, the coefficient of determination between TSM_trg and a_g was 0.86 [14]. In the

coastal zone, the coefficient of determination between b_{bp} and a_g was 0.82, whereas, in the open part, it was close to 0. The average value of a_g in the open part was 0.098 m^{-1} as compared to 0.13 m^{-1} in the coastal zone. As for the background values, the lowest monthly mean of a_g , derived from satellite data over 2003–2010, was equal to 0.047 m^{-1} with the standard deviation of 0.013 m^{-1} (range: $0.021\text{--}0.060 \text{ m}^{-1}$) [14].

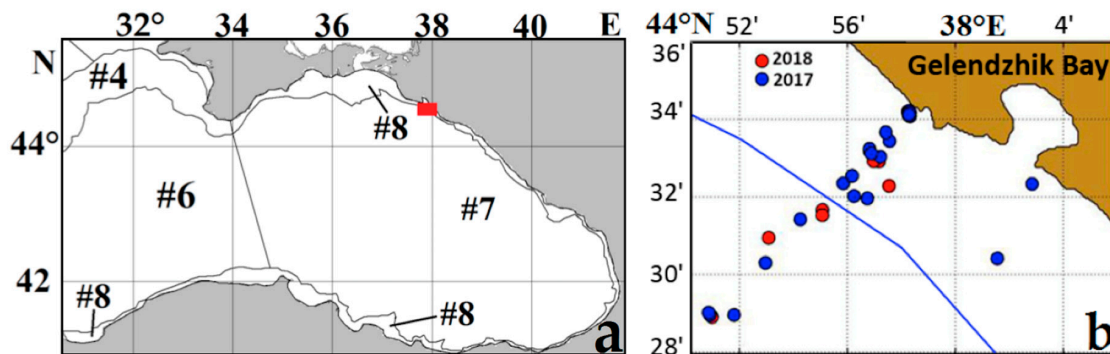


Figure 1. The study areas: (a) sub-regions: #4—northwestern outer shelf; #6—western open part; #7—eastern open part; #8—eastern and southern shelves [19,20]; (b) location of the drift stations in 2017 (blue) and 2018 (red); the blue line is the border between sub-regions #7 and #8.

Direct measurements of the spectral absorption coefficients $a_g(\lambda)$ were conducted since 2017 with a portable spectrophotometer in the integrated cavity absorption meter (ICAM) configuration, developed at the Department of Biophysics, Biological Faculty, Moscow State University [21]. Its description is given in the next section. Measurements were carried out on samples taken from different horizons at drift stations. The stations were located at depths of 25–100 m in the shallow-water part and 500–1500 m in the deep-water part (Figure 1b); for more details, see Reference [22].

In this paper, we focus on the results of 2017–2018; the analysis is based on both satellite and in situ data (see the next section). These years are quite different in their oceanographic and hydrometeorological conditions; in particular, in 2017, the most intensive CB within the whole period of studies was observed, whereas there was no pronounced CB in 2018. The research highlight of our work is an explanation of the unusual situation concerning the CDOM absorption in 2018, namely, high CDOM absorption under elevated values of salinity. This means that the river runoff is not a main source of CDOM as mentioned above, and an alternative source should be found. To be sure of the appropriate quality of the measurement data, we compared the values of a_g derived from different measurements. To obtain a more complete picture of the influence of various factors, the available data from previous years were also analyzed.

2. Materials and Methods

2.1. In Situ Studies

2.1.1. Measurements of the Spectral Absorption Parameters

Spectral seawater absorption coefficients were obtained using a portable spectrophotometer in the ICAM configuration, developed at the Department of Biophysics, Biological Faculty, Moscow State University, Moscow, Russia [21].

The so-called ICAM (integrated cavity absorption meter) technologies, named so because the studied water is placed inside the integrating sphere, were actively developed in the past two decades. The use of such an approach allows avoiding problems associated with light scattering (see Section 1) and increasing sensitivity due to the multiple reflections of light inside a sphere. However, for the determination of the absolute values of the absorption coefficient, it is necessary to know the effective path length of photons, taking into account their multiple reflections. This problem was studied,

and a special algorithm with a processing program was developed. The Monte Carlo calculations performed showed that the results of the determination of the absorption coefficient are independent of the seawater scattering properties when the scattering coefficient b varies from 0 to 5 m^{-1} [23].

Three measurements of the absorption spectrum were taken for each water sample: (1) seawater; (2) after filtration through the nuclear filter of $0.4 \mu\text{m}$ (absorption spectra of the filtrate); (3) the empty sphere. The spectral absorption coefficient of seawater (or the filtrate) was calculated through the ratio of the measured spectral dependencies for the sphere filled with the sample to the empty sphere [23]. Distilled water spectra were recorded in the control tests. The volume of the water sample was 330 mL; replicate samples were collected and measured for each series of measurements. The absorption spectra of the particles were not measured but determined as a difference between the spectral values of the seawater absorption and of the filtrate absorption. A detailed description of the measurement procedure and calculation is given in Reference [23].

2.1.2. Measurements of the Vertical Structure

A conductivity, temperature, and depth (CTD) profiler with the “SBE 19+, Seacat” sampling system was used to measure the vertical distributions of the following hydrological parameters: salinity, temperature, density, and chlorophyll fluorescence (F_{chl}). To measure the vertical distribution of the light attenuation coefficient, a submersible transparency meter [24] was used.

In accordance with the features of the vertical structure, water samples at each station were taken from 4–5 selected depths for study in an onshore laboratory. The laboratory measurements included the absorption spectra by the ICAM instrument, determination of concentrations of chlorophyll, suspended matter, phytoplankton content, and species composition. These studies were performed according to standard procedures [14].

Direct measurements of the depth dependence of spectral underwater irradiance $E_d(z, \lambda)$ created by the downwelling flux of solar radiation were performed using a RAMSES hyperspectral radiometer (model ACC-VIS), manufactured by TriOS Optical Sensors, Germany. The radiometer is designed to instantaneously measure spectral irradiance at wavelengths from 320 to 950 nm with a 3-nm resolution down to a depth of 100 m. The dynamic range of the irradiance channel is $3\text{--}0.003 \text{ W}\cdot\text{m}^{-2}\cdot\text{nm}^{-1}$. A special frame was constructed for properly submersing the instrument; the data were transmitted via cable to a laboratory unit. A notebook computer was used to record and process the data. The radiometer was calibrated by the TriOS company in compliance with National Institute of Standards and Technology (NIST) specifications. The measured $E_d(z, \lambda)$ values allowed us to compute the diffuse attenuation coefficients for underwater irradiance, $K_d(\lambda)$ under the assumption that irradiance attenuation with depth obeys the exponential law $E_d(z) = E_d(0^-) \exp[-K_d z]$, where wavelength λ is omitted for simplicity.

2.2. Calculation of Hydrometeorological Parameters

Calculations of precipitation and wind characteristics were carried out on the basis of data from the ERA-Interim (European Interim Reanalysis) reanalysis archive using the ECMWF model (European Center for Medium-Range Weather Forecasts) with a 12-hour time step and a spatial resolution of 0.125×0.125 degrees, available at the website [25]. These models were used to calculate daily spatial distributions from 1 April to 11 June (the expedition end date) 2010–2018 in the region of $44.2^\circ\text{--}44.8^\circ$ north (N), $37.5^\circ\text{--}38.5^\circ$ E.

To assess the river discharge in this part of the Black Sea, data from an automated flood situation monitoring system in the Krasnodar region, available at the website [26], were used. Unfortunately, most of the posts provided only data on the water level in the rivers in the Baltic height system. We used data for the Ashamba River (Yashamba), the closest to the area of the field studies, flowing into Rybachya (Blue) Bay, and Mzymta, a deep river in the region under consideration, fasting station AGK-0160 (43.517° N, 39.996° E). The measurement data were obtained with an interval of 10 min; in constructing the graphs, the running average method with an averaging interval of one day was used.

2.3. Satellite Observation Data

On the National Aeronautics and Space Administration (NASA) website [27], the parameters of our interest are freely available, but most of them are calculated using empirical (regression) or semi-analytical algorithms [19,28]. Most of these algorithms were developed by using data from field measurements mainly for ocean waters. In waters that are strongly influenced by river runoff, such as the waters of the Black Sea, the standard algorithms can produce large errors [19]. Thus, in such seas, it is necessary to use regional algorithms to obtain correct data on bio-optical parameters. These algorithms were developed on the basis of data from the field measurements in the studied regions, taking into account their features. Validation studies performed in SIO RAS expeditions showed that the use of regional algorithms can significantly reduce errors of the satellite estimation, compared to standard algorithms.

The algorithms used in this work are described in detail in Reference [19] and on the website [20]. They allow to calculate the chlorophyll concentration Chl , the particle backscattering coefficient b_{bp} , and the absorption coefficient of yellow substance a_g ; the special regional algorithms were developed to derive concentrations of the chlorophyll, suspended matter, and coccolithophore cells during the mass blooming period which usually occurs in June [14,19,20].

We used the Level 2 data of satellite spectroradiometers Moderate-Resolution Imaging Spectroradiometer (MODIS)-Aqua and MODIS-Terra, available through the NASA website [27]. These are the values of geophysical parameters calculated after atmospheric correction, corresponding to the initial pixels, i.e., with the same coordinate and time values as the original values. The five-day averages were calculated for the spatial distribution of the values of a_g , Chl , and TSM in May and June 2017–2018. The monthly average values of these characteristics and sea surface temperature were estimated for the period of 2012–2018. The calculation was performed with a spatial resolution of 2×2 km for five-day averages and 3×3 km for monthly averages by using software [29] developed in the Laboratory of Ocean Optics SIO RAS, Moscow, Russia. Data marked as land, clouds, and stray light flags were excluded.

The above-mentioned package includes programs for maintaining the database, which contains files from satellite and ship measurements, programs for batch processing of large amounts of satellite data, and a host program for visualizing satellite and ship data, as well as for launching other components of the program complex. A set of programs for batch processing of satellite files contain modules for calculating new products and recording results in HDF (Hierarchical Data Format), and NetCDF (Network Common Data Form) formats, averaging data, constructing maps in a given projection, creating time series, etc. Features of the programs of this system are the dynamic loading of libraries that can be developed by users and implemented without recompilation of programs, and the presence of a convenient and fairly universal language for task management [19].

3. Results

3.1. Satellite Data

Figure 2 shows the changes in monthly mean values of the yellow substance absorption coefficients a_g and the particle backscattering coefficients b_{bp} in the #7 and #8 sub-regions (see Figure 1) derived from MODIS-Aqua data of 2012–2018 by using the SIO RAS regional algorithms. The black lines show the seasonal variability of the “climatic” values which are averaged values over the period of 1998–2011. One can see the pronounced inter-annual variability of the bio-optical parameters compared with the seasonal variability of the climatic values. Our purpose is to identify the causes of the observed variability, primarily for the yellow substance absorption coefficients a_g . The solution to this problem is possible only on the basis of in situ measured data and an analysis of factors that determine the seasonal and inter-annual variability of bio-optical and hydrometeorological characteristics.

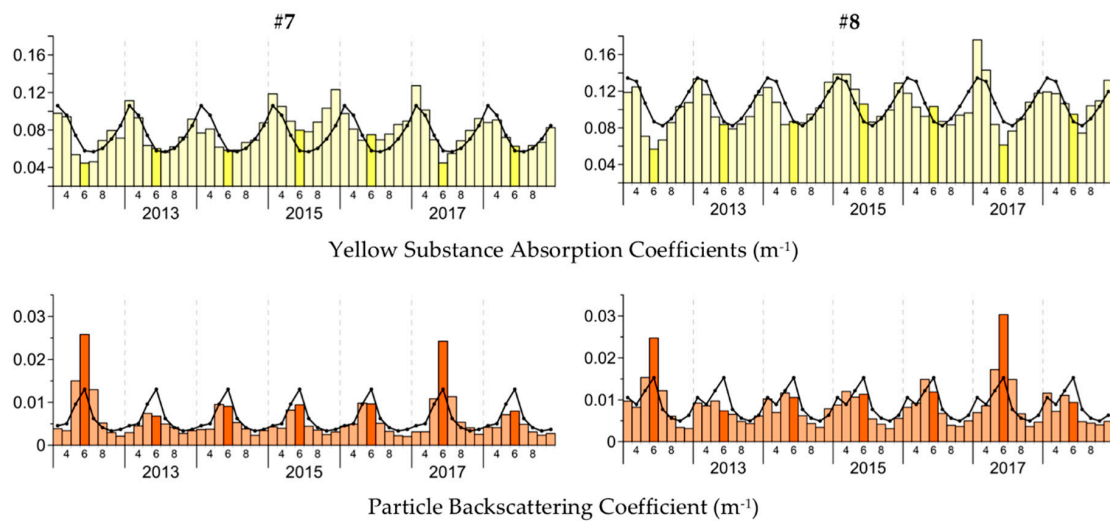


Figure 2. Variability of the monthly mean values of the yellow substance absorption coefficients a_g and the particle backscattering coefficients b_{bp} in the eastern open part (sub-region #7) and in the eastern and southern shelf areas (sub-region #8) of the Black Sea in 2012–2018. The black lines show the seasonal variability of the climatic values, which are averaged values over the period of 1998–2011.

We are mainly interested in data for June when our field studies were carried out, as well as, of course, the above area itself. Thus, we limited the representation of satellite data mainly to this area (see Figure 1) and considered the dynamics of the changes during the period when these studies were conducted. Figure 2 clearly demonstrates that the seasonal and inter-annual changes in the monthly means of a_g and b_{bp} are quite different. In particular, the June monthly means of a_g were larger than the climatic values in 2015, 2016, and 2018, whereas the b_{bp} values in these years were lower. This certainly indicates that the variability of a_g and b_{bp} is controlled by different factors.

Figure 3 shows the spatial distributions of the yellow substance absorption coefficient a_g and the particle backscattering coefficient b_{bp} from MODIS data averaged over five days from 1 June to 15 June 2017 and 2018. One can see that the years 2017 and 2018 sharply differed from each other. In 2017, high values of b_{bp} but low values of the yellow substance absorption coefficient a_g were observed. In 2018, on the contrary, markedly higher values of the yellow substance absorption coefficients were observed, especially near the coast, along with lower b_{bp} values.

The reason for elevated values of the particle backscattering coefficients b_{bp} is known; CB of very high intensity was observed in June 2017. Figure 4 shows the spatial distributions of the coccolithophore concentration, calculated from MODIS-Aqua data on 5 June and 8 June 2017, using the SIO RAS algorithm [14]. As seen, in both days, the concentration of cells in the coastal zone in the area of our work exceeded 8×10^6 cells/L.

The difference in the values of the particle backscattering coefficients b_{bp} in 2017 and 2018 was strongly pronounced in the satellite observation under clear sky conditions. It is clearly seen from the comparison between the values of the spectral remote-sensing reflectance $R_{rs}(\lambda)$ measured by the MODIS-Aqua sensor in 2017 and 2018 (Figure 5). It is also seen that the difference between shallow-water and deep-water stations was rather small in 2018 and higher in 2017.

On 8 June, the full-scale *in situ* measurements were carried out and the samples were taken to determine the quantitative and species composition of phytoplankton. The coccolithophore cell concentration in the coastal zone turned out to be approximately the same as that from the satellite data, i.e., about 8×10^6 cells/L.

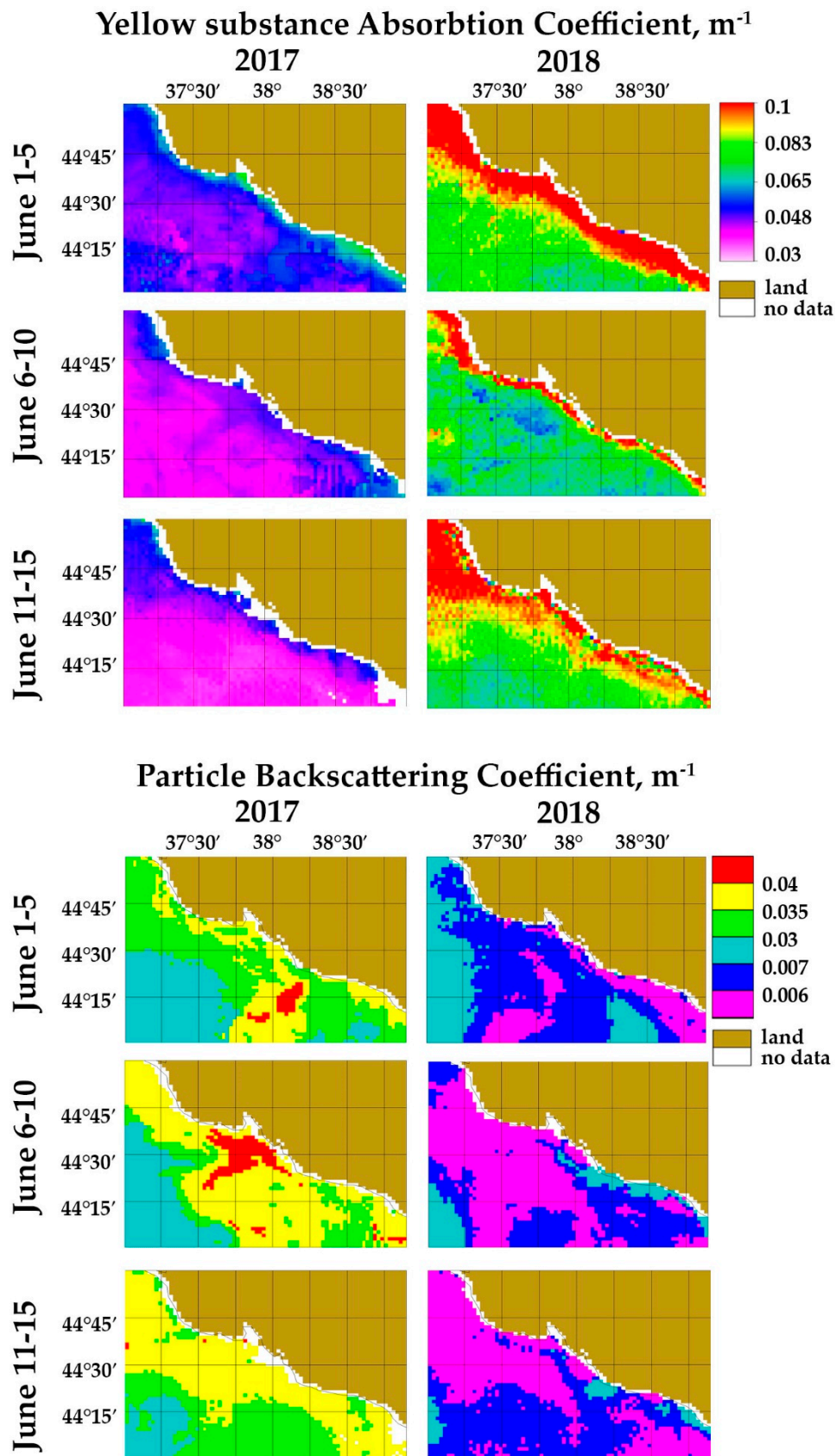


Figure 3. The spatial distributions (from top to bottom) of values of the yellow substance absorption coefficients a_g and particle backscattering coefficients b_{bp} derived from Moderate-Resolution Imaging Spectroradiometer (MODIS)-Aqua data of 1–15 June 2017 and 2018.

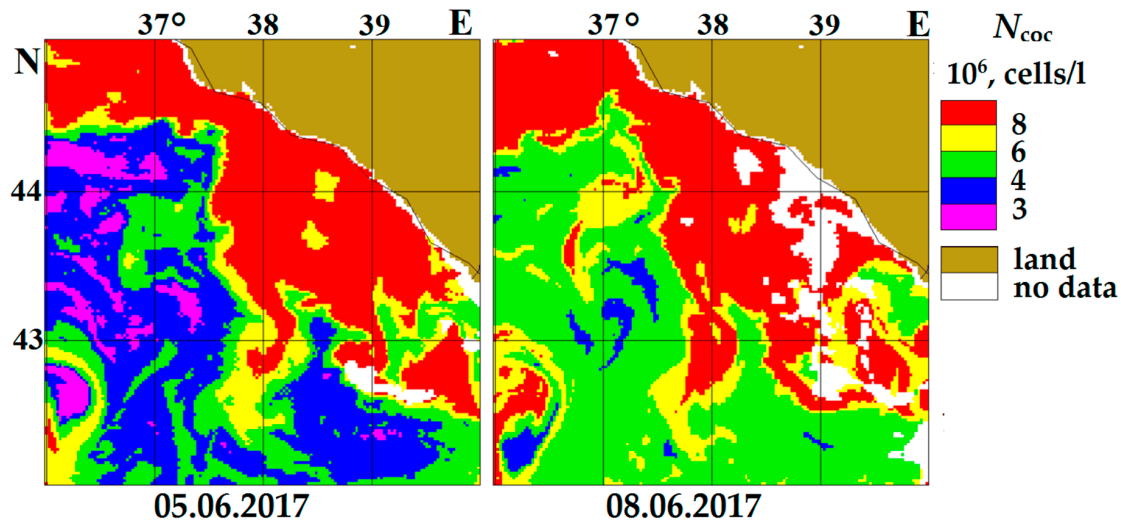


Figure 4. The spatial distributions of the coccolithophore concentration N_{coc} values (plated cells) derived from MODIS-Aqua data on 5 and 8 June 2017.

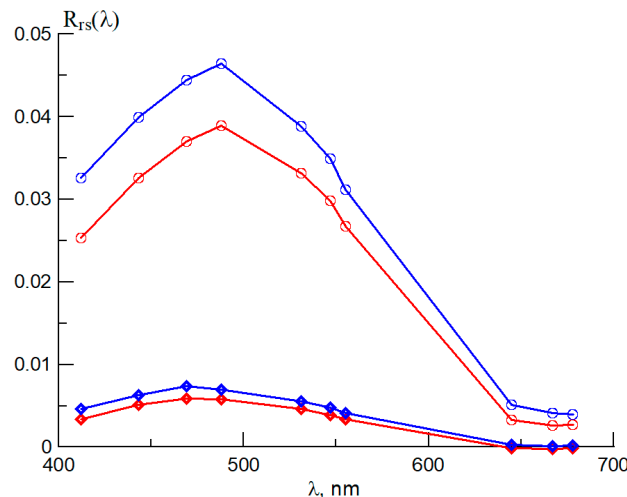


Figure 5. Spectral remote-sensing reflectance $R_{rs}(\lambda)$ from MODIS data measured over deep-water (blue lines) and shallow-water (red) stations in 2017 (circles) and 2018 (diamonds). The stations were located at depths of 50 and 1500 m in 2017 (June 8) and 2018 (June 9).

3.2. Spectral Absorption Measurements on the ICAM

In Section 1, we mentioned an unusual situation concerning the CDOM absorption in 2018, namely, high CDOM absorption under elevated values of salinity. Here, we try to show this situation in detail and understand which additional information is required to explain the results obtained.

Figure 6a shows the absorption spectra of the filtrate (a_f), and Figure 6b shows the suspended particles (a_p), measured in the surface layer at three shallow-water stations in 2017, 2018, and 2019. As seen, the highest absorption by the filtrate was observed in 2018, and by suspended particles in 2017, where the latter is obviously associated with intensive CB.

Recall that the absorption spectra of particles were obtained as a difference between the spectral values of the absorption coefficient of seawater before and after filtration through a filter with a pore size of $0.4 \mu\text{m}$. As seen from Figure 6b, the absorption spectra of particles in all years expose the maxima caused by phytoplankton pigments: the blue maximum at 430–440 nm, the shoulder near 480 nm due to absorption by carotenoids, and the red maximum at 675–680 nm caused by chlorophyll absorption. This suggests that most suspended particles, the sizes of which exceed $0.4 \mu\text{m}$, are of biological origin.

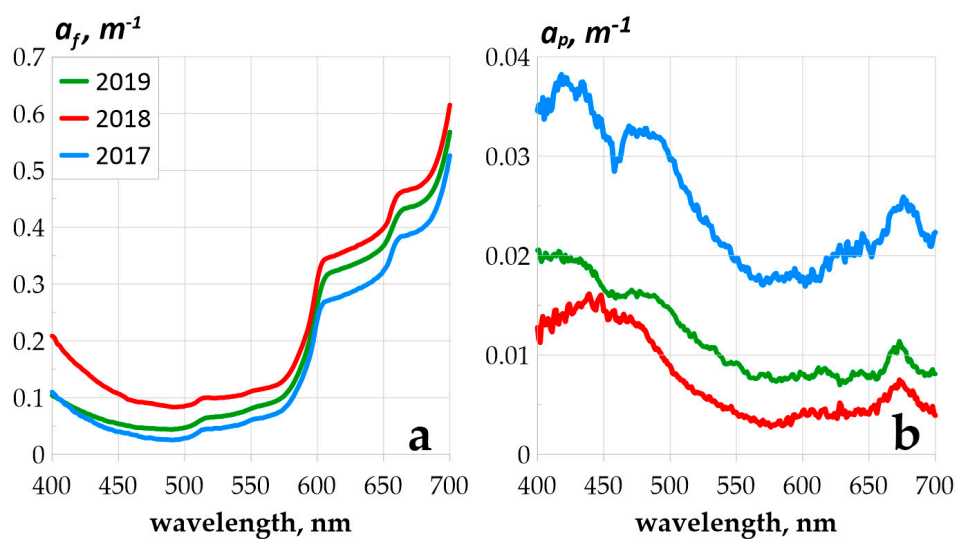


Figure 6. Absorption spectra of the filtrate (a) and suspended particles (b) for three stations in 2017–2019 measured by integrated cavity absorption meter (ICAM).

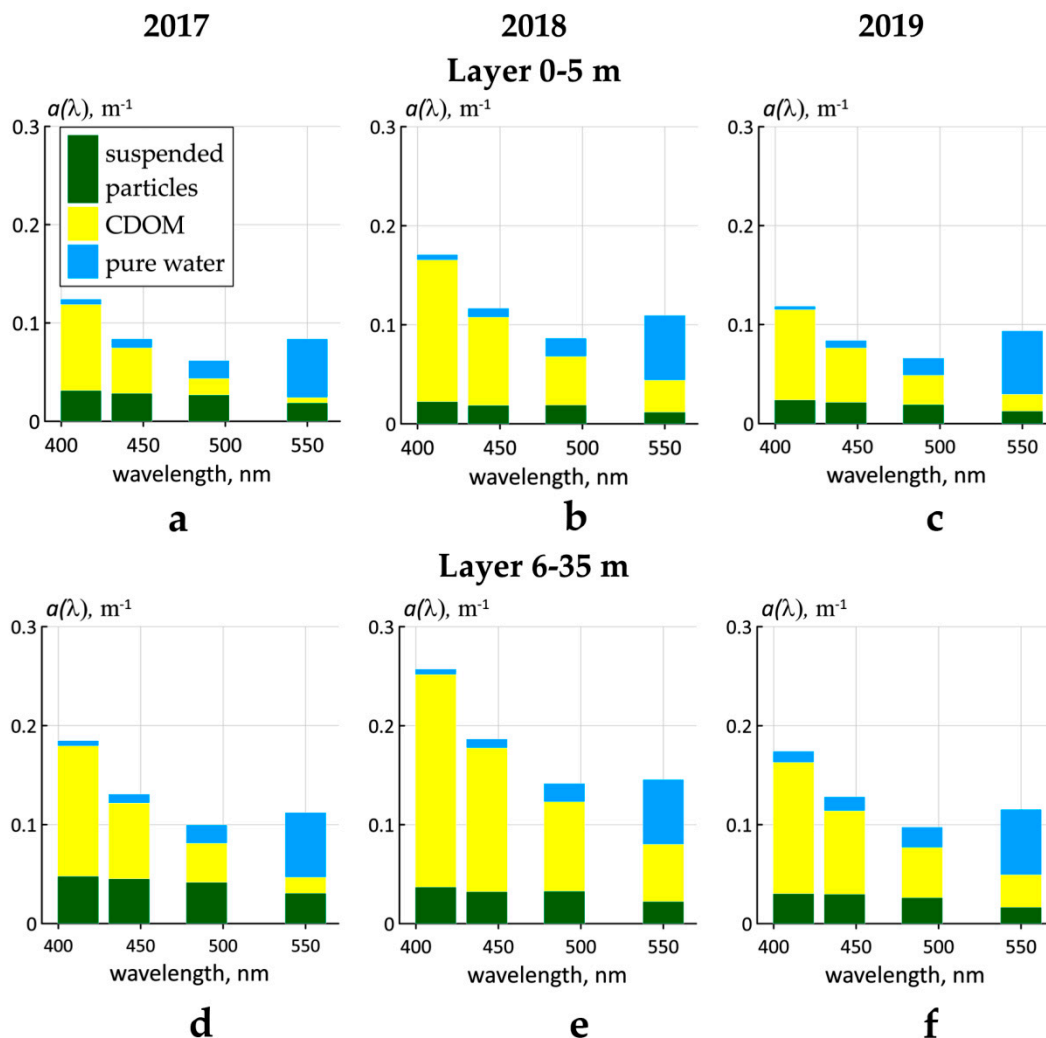


Figure 7. Contributions from the suspended matter, colored dissolved organic matter (CDOM), and pure water in the total seawater light absorption: (a–c) the layer from 0–5 m; (d–f) the layer from 6–35 m. Values are shown for 2017 (a,d), 2018 (b,e), and 2019 (c,f).

The average values of contributions to the seawater light absorption from the CDOM and suspended particles at the wavelengths corresponding to the spectral channels of MODIS in the layers at 0–5 m and 6–35 m are shown in Figure 7. It is seen that the highest values of the seawater absorption coefficients were recorded in 2018, due to the increased CDOM absorption. The higher (about twofold) values of the particle absorption coefficient a_p were recorded in 2017 under conditions of strong CB. In 2019, absorption values were close to those observed in 2017, but with less particulate absorption than in 2017 and less CDOM absorption than in 2018. The inter-annual differences are also observed in the underlying layers, even more pronounced than in the surface layer.

One should pay attention to absorption in the underlying layer of 6–35 m; in all years, it was noticeably higher than in the subsurface layer of 0–5 m. Next, we turn to this observation.

3.3. Comparison between the a_g values derived from different measurements

Comparison of the values of the yellow substance absorption coefficient measured by the ICAM and calculated from MODIS-Aqua and MODIS-Terra satellite data using the SIO RAS algorithm showed good agreement between them (Figure 8): coefficient of determination $r^2 = 0.63$ (correlation coefficient $r = 0.79$), number of pairs $n = 35$, average relative error = 17%, mean square error SD = 0.016 m^{-1} ; these values are comparable with the errors of field measurements.

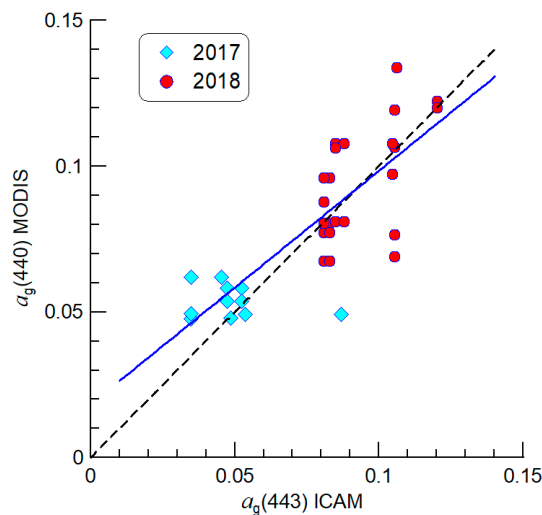


Figure 8. Scatterplot of the $a_g(443)$ values, calculated from satellite MODIS data, relative to the values measured by ICAM.

Table 1 presents results of the comparison between the values of $a_g(443)$ measured by ICAM and those calculated using MODIS data on the remote-sensing reflectance R_{rs} and from data of K_d measurements in 2018.

Table 1. The values of $a_g(443)$ measured by integrated cavity absorption meter (ICAM), and calculated according to Moderate-Resolution Imaging Spectroradiometer (MODIS) (R_{rs}) and light measurements (K_d) in 2018. The relative error (%) is indicated in parentheses.

Station	ICAM	MODIS (R_{rs})	From K_d
At depth of 50 m	0.081	0.076 (−6%)	0.074 (−9%)
At depth of 1500 m	0.085	0.111 (+30%)	0.066 (−22%)

The spectral diffuse attenuation coefficient K_d in the near-surface layer (0–10 m) was calculated from the measured values of the downwelling spectral irradiance. Furthermore, the sum of the absorption and backscattering coefficients was computed using Gordon’s formula [30]. The particle backscattering coefficient $b_{bp}(555)$ was determined from satellite data using the algorithm in Reference [31]; then, the

spectral particle backscattering coefficient was calculated using the following formula: $b_{bp}(\lambda) = b_{bp}(555) (555/\lambda)^{0.5}$. The data in Reference [32] were used for backscattering by pure seawater. As a result, the estimates for the spectral coefficient of seawater absorption were obtained, which are in good agreement with the measurement data. For 2017, no calculations were carried out, since Gordon’s formula gives big errors for conditions of strong CB (this formula was derived with quasi-single scattering approximation [30]).

From Table 1, it is seen that the K_d measurements give smaller errors than those from MODIS data. In the first case, the difference is within 9–22%; in the second, the error varies from –6% to +30%.

3.4. Comparison of Optical and Hydrological Data

Table 2 presents the average values of the main parameters measured in situ in 2017 and 2018 and averaged over three layers of different depths; these are the yellow substance absorption coefficient, salinity, temperature, chlorophyll concentration, and the beam attenuation coefficient c for shallow-water (station depth 25–80 m) and deep-water stations (more than 300 m), averaged over three layers.

Table 2. Average values of various parameters, their standard deviations at different horizons, and the number of values for calculation (in parentheses). *Chl*—chlorophyll concentration; *F_chl*—chlorophyll fluorescence.

Shallow Water						
Depth, m	a_g (m^{-1})	S (psu)	T ($^{\circ}C$)	<i>Chl</i> ($mg \cdot m^{-3}$)	N_{coc} ($\times 10^6$ Cells/L)	c (m^{-1})
2017						
Above	0.10 ± 0.02 (11)	17.1 ± 0.2 (23)	21.3 ± 1 (23)	0.66 ± 0.3 (23)	6.7 ± 2 (23)	2.3 ± 0.2 (23)
Maximum <i>F_chl</i> (8–17 m)	0.13 ± 0.02 (9)	18.0 ± 0.2 (12)	14.2 ± 1 (12)	2.1 ± 0.7 (12)	7.0 ± 2.3 (12)	2.3 ± 0.4 (12)
Below	0.13 ± 0.03 (3)	18.3 ± 0.1 (13)	10.3 ± 1 (13)	1.02 ± 0.3 (13)	0.57 ± 0.7 (13)	0.8 ± 0.3 (13)
2018						
Above	0.16 ± 0.03 (10)	17.8 ± 0.1 (10)	22.7 ± 1 (10)	0.3 ± 0.03 (5)	0.51 ± 0.1 (4)	0.70 ± 0.1 (10)
Maximum <i>F_chl</i> (17–21 m)	0.25 ± 0.02 (4)	18.1 ± 0.1 (4)	15.3 ± 0.7 (4)	2.08 ± 0.9 (4)	0.46 ± 0.3 (4)	1 ± 0.1 (4)
Below	0.16 ± 0.04 (5)	18.3 ± 0.1 (5)	11.6 ± 1 (5)	1.72 ± 0.3 (2)	0.20 ± 0.2 (2)	0.5 ± 0.2 (5)
Deep Water						
Depth, m	a_g (m^{-1})	S (psu)	T ($^{\circ}C$)	<i>Chl</i> ($mg \cdot m^{-3}$)	N_{coc} ($\times 10^6$ cells/L)	c (m^{-1})
2017						
Above	0.07 ± 0.01 (5)	17.2 ± 0.2 (8)	21.7 ± 1 (8)	0.5 ± 0.15 (8)	6.3 ± 1.6 (8)	2.6 ± 0.1 (8)
Maximum <i>F_chl</i> (8–17 m)	0.16 (1)	18.2 ± 0.1 (4)	12.4 ± 0.8 (4)	1.06 ± 0.5 (4)	6.4 ± 3.1 (4)	1.8 ± 1 (4)
Below	0.13 ± 0.02 (3)	18.3 ± 0.1 (6)	8.7 ± 0.9 (6)	0.92 ± 0.6 (6)	0.1 ± 0.07 (6)	0.4 ± 0.1 (6)
2018						
Above	0.16 ± 0.04 (14)	17.6 ± 0.2 (14)	22.3 ± 1 (14)	0.35 ± 0.2 (6)	0.8 ± 0.30 (4)	0.7 ± 0.1 (14)
Maximum <i>F_chl</i> (17–21 m)	0.26 ± 0.05 (4)	18.1 ± 0.1 (5)	14.5 ± 1 (5)	2.03 ± 0.3 (5)	0.7 ± 0.43 (5)	1.2 ± 0.2 (5)
Below	0.18 ± 0.03 (6)	18.3 ± 0.1 (5)	11 ± 1.3 (5)	1.06 ± 0.3 (2)	0.22 (1)	0.4 ± 0.1 (5)

The values of the yellow substance absorption coefficient a_g and the salinity S in the subsurface layer are highlighted in red. It is seen that, in 2018, the selected values of a_g were larger than in 2017 both in the shelf zone and in the open sea. It is noteworthy that the values of salinity were also greater. This is an unusual situation because it is generally accepted that the CDOM concentration is associated with river runoff, and its increase must be accompanied by a decrease in salinity.

Figure 9 shows the daily averaged profiles of salinity, temperature, and chlorophyll from the CTD fluorescence sensor, and the beam attenuation coefficient from a transparency meter, separately for shallow-water and deep-water stations in 2017 and 2018.

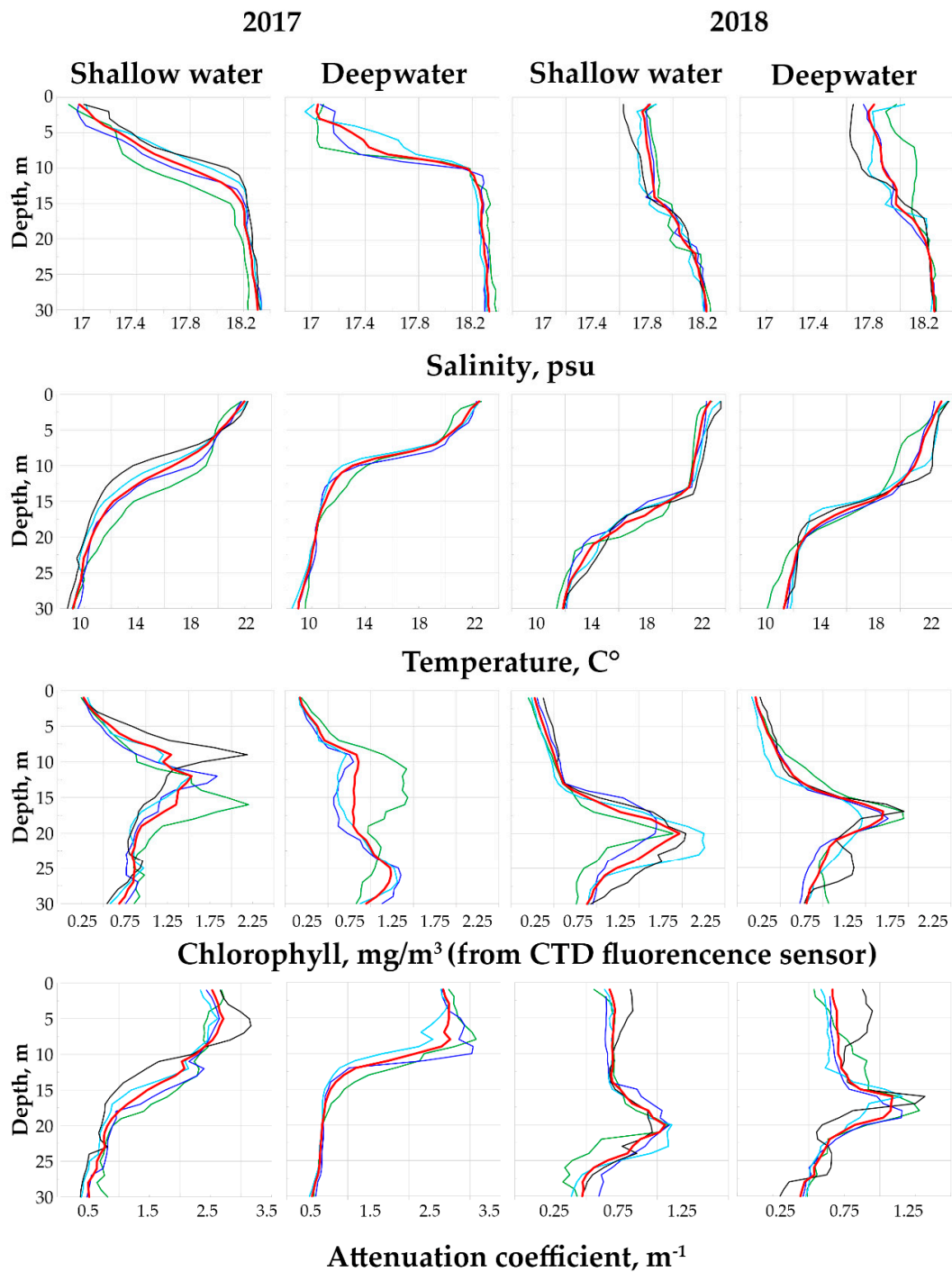


Figure 9. Daily profiles of the main characteristics for shallow-water (25–80 m) and deep-water (from 300 to 1500 m) stations. The averaged profiles are shown in red. The data obtained in 2017 were for 8 June (green), 9 June (blue), 10 June (cyan), and 11 June (black); the data obtained in 2018 were for 5 June (green), 6 June (blue), 8 June (cyan), and 9 June (black).

The difference in the attenuation coefficient $c(z)$ is primarily due to the CB in 2017 increasing the scattering; the maximum $c(z)$ was at the surface layer, where the maximum N_{COC} usually lies. The thermocline, like the maximum fluorescence, was deeper in 2018 than in 2017. There is a sharp distinction observed between the vertical salinity profiles in 2017 and 2018 both in shallow-water and deep-water stations. If, in 2017, the differences in salinity on the surface and below 15 m were about 1 psu, then, in 2018, these differences were only about 0.4 psu. It can be assumed that the observed

differences are associated with different hydrometeorological conditions in 2017 and 2018, and, to test this assumption, we examined precipitation, wind, and river levels.

4. Discussion

The results of our field studies in 2017 and 2018 with the involvement of satellite data revealed an unusual situation in 2018 as compared with 2017, namely, the elevated values of the CDOM absorption coefficient a_g concurrently with higher values of salinity in the surface layer. This is in contradiction with the accepted idea that the main source of CDOM is the river runoff and that, therefore, the increased values of the CDOM absorption should be accompanied by lower values of salinity. In this section, the various factors are discussed to understand which of them can potentially affect the situation.

4.1. Interannual Salinity Measurements

Variability of salinity in the upper layer in Gelendzhik region of the Black Sea during the warm season in 2010–2013 was studied, together with analysis of coastal precipitation and wind forcing, by Podymov and Zatsepin [22]. They demonstrated the pronounced anomalies in salinity in the layer of 0–5 m, especially in June 2011 when the salinity values in the deep part of the region decreased below 16 psu as compared with about 17.7 psu in June 2013.

We calculated changes in salinity in the layers of 0–5 m and 6–35 m within the period of 2013–2018 by using the data measured in our field studies. The results presented in Figure 10 also show the pronounced decreases in salinity in 2014 and 2017, and its highest values were observed in 2018 (our values for the layer of 0–5 m in 2013 are in good agreement with Reference [22]).

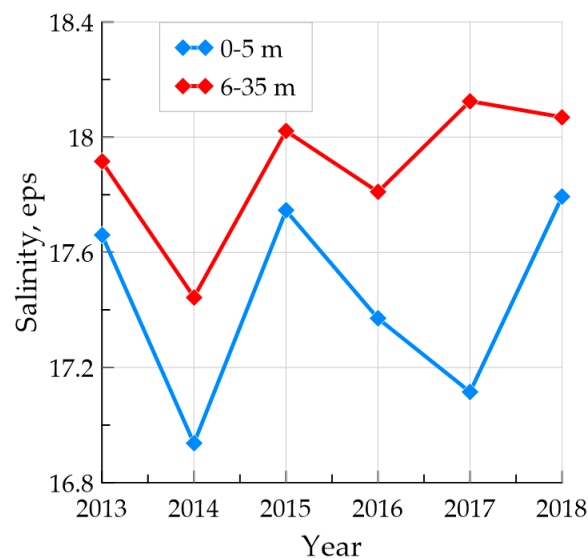


Figure 10. Changes in salinity in the layers of 0–5 m and 6–35 m within the period of 2013–2018 (from our field studies in June).

It is seen from Table 2 and Figure 9 in the previous section that, in 2018, the salinity in the upper 5-m layer in the shelf zone was even higher than in 2013—about 17.8 psu (in 2017, it was slightly higher than in 2011). Looking ahead, we note that precipitation in 2018 was lower than in 2013 (from 1 April to 11 June, 0.68 mm and 0.83 mm, respectively); in 2017, it was also lower than in 2011—1.89 and 2.00 mm, respectively (Table 3).

According to the results obtained in [22], high salinity values in June 2013 are primarily associated with precipitation or, rather, their absence; in 2013, the total precipitation at the beginning of May was 1.5 times less than in 2010–2011 (214 mm), and this trend continued in June. According to Reference [22],

the effect of wind variability on surface salinity was not noticeable; however, generally speaking, this effect can be significant, since its impact is proportional to the third power of wind speed.

Table 3. Average and total precipitation for the period from 1 April to 11 June 2010–2018.

Year	2010	2011	2012	2013	2014	2015	2016	2017	2018
Precipitation (mm)	1.00	2.00	1.13	0.83	1.47	1.52	1.57	1.89	0.68
ΣPrecipitation (mm)	72.0	144.2	81.1	59.5	105.6	109.7	113.1	136.4	48.8

At a depth of 30 m, salinity was approximately 18.2 psu in both 2017 and 2018 (see Figure 9), but there are noticeable differences in the upper 15-m layer between 2017 and 2018. Pay attention to the change in the lower depth of the halocline; in 2017, it was about 13 m; in 2018, it increased to 15 m.

4.2. Precipitation and Wind

Figure 11 shows the daily precipitation from 1 April to 11 June (the end of the expedition) 2010–2018 and the monthly mean precipitation, summarized over the catchment area (see Figure 12); numerical values are given in Table 3. These values were obtained from data of the ERA-Interim reanalysis archive (European Interim Reanalysis), using the ECMWF model (European Center for Medium-Range Weather Forecasts).

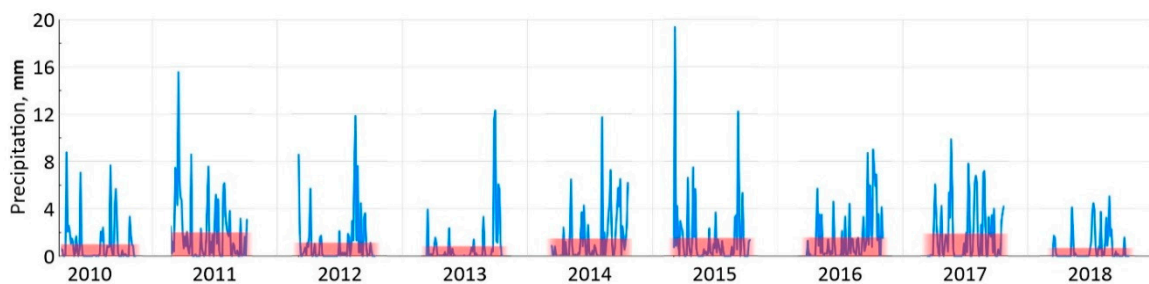


Figure 11. The daily (blue lines) and average monthly (pink bar diagrams) precipitation from 1 April to 11 June 2010–2018.

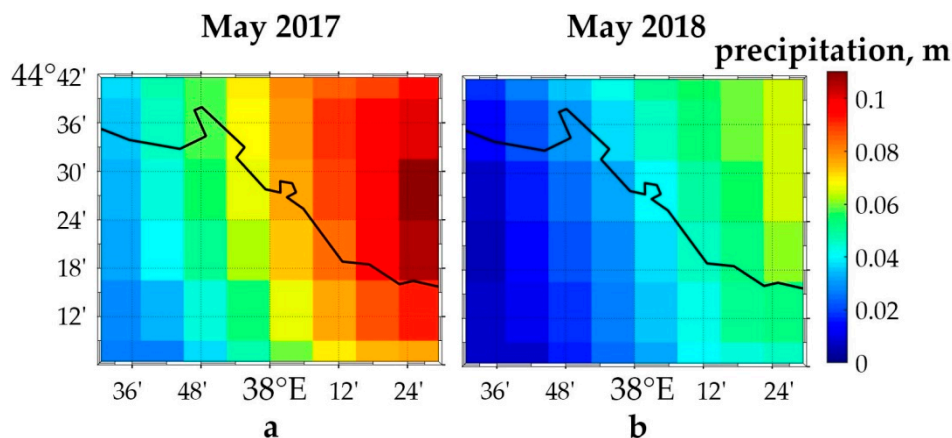


Figure 12. Distribution of average daily precipitation values in the catchment area in the period from 1 May to 31 May 2017 (a) and 2018 (b).

Figure 13 shows how the water level in the Ashamba and Mzymta rivers changed during April–June 2017–2018. For both rivers, the water level in 2017 was significantly higher than in 2018 by an average of 20–30 cm, which corresponds to the estimates of the total precipitation for the area under consideration, which was more in 2017.

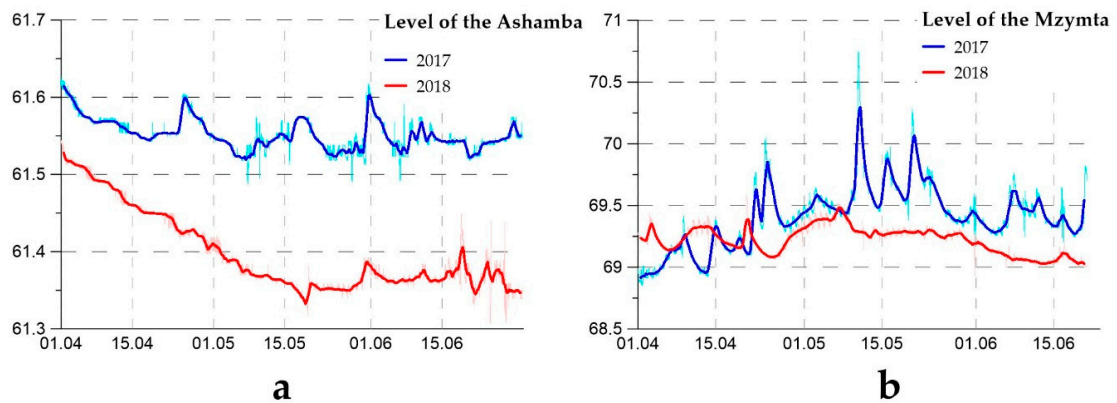


Figure 13. Changes in water level during April–June 2017–2018 in the rivers Ashamba (a) and Mzymta (b). Thin lines represent measurements every 10 min, whereas thick lines represent averages with one-day intervals.

Comparing Figures 11 and 13, one can see that the maxima of the water level in the rivers often correspond to the maximum precipitation. For example, in 2017 three well-seen maxima of precipitation (9, 16, and 23 May) are also displayed on the graph of changes in water level in the Mzymta River. For the Ashamba River during this period, an increase in water level is seen only on 16–17 May, which is consistent with the distribution of precipitation in the region.

Figure 14 presents the values of the third degree of wind speed according to ECMWF ERA-Interim reanalysis, averaged over the area at a height of 10 m, which is proportional to the magnitude of wind exposure. The average wind speed from 1 May to 11 June was 3.5 m/s in both 2017 and 2018, but the highest value (10.7 m/s) was observed on 29 May 2018 (Figure 14) and the total wind exposure in 2018 was significantly higher than in 2017—more than 4000 m³/s³ and less than 3000 m³/s³, respectively. The weakest wind effect was observed in 2011—about 1650 m³/s³.

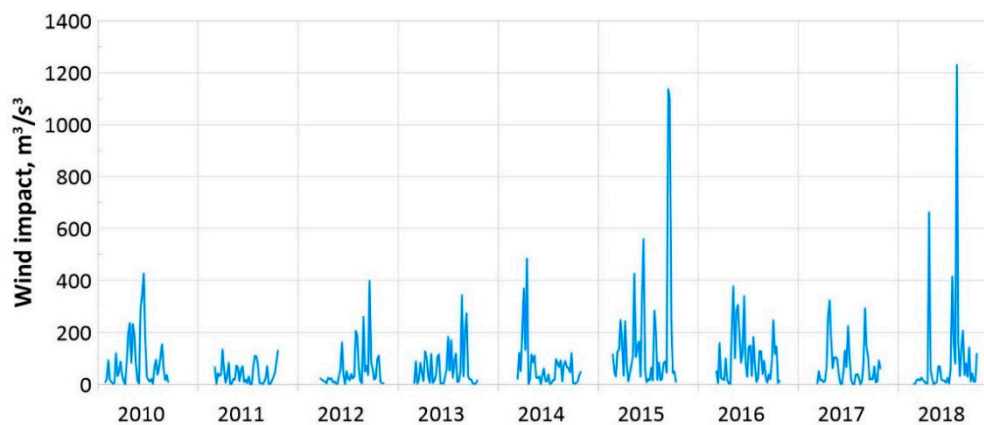


Figure 14. The average wind impact on the considered area from 1 May to 11 June 2010–2018.

4.3. Main Results and Conclusion

In 2017 and 2018, comprehensive bio-optical studies were carried out in the northeastern part of the Black Sea (near Gelendzhik), including direct measurements of the seawater spectral absorption coefficients by means of a portable spectrophotometer. An unusual situation was observed in 2018, when elevated values of the CDOM absorption in the surface layer were accompanied by a high value of salinity. This means that the river runoff is not the only source of yellow substance in the surface layer, as it is considered at present.

Comparison between vertical profiles of salinity in 2017 and 2018 found not only an increase in salinity in the upper 5-m layer but also a change in the shape of a vertical profile—a violation of

the pronounced vertical stratification, which was in 2017, and erosion of the halocline, lowering its lower boundary. If the increase in salinity in the upper 5-m layer can be explained by a decrease in precipitation in 2018 (the smallest amount from 1 April to 11 June in the period 2010–2018), the change in underlying layer suggests that it was due to vertical mixing.

A thorough analysis of changes in salinity in a given area under the influence of various factors was presented in Reference [22]. One of the factors could be wind forcing. However, in 2010–2013 (the period considered in Reference [22]), the wind was weak and the wind forcing was hardly noticeable. In 2018, the wind forcing increased dramatically—about 1.5 times compared to 2013 (Table 4), and this suggests that, in 2018, a strong wind forcing was the main factor behind the increasing values of salinity and a_g in the surface layer.

Table 4. Wind exposure in the period 2010–2018: top row—the averaged values of V^3 , bottom—the integrated value of V^3 over the total area.

Year	2010	2011	2012	2013	2014	2015	2016	2017	2018
Average V^3 (m^3/s^3)	85.2	39.3	55.6	63.2	69.5	163.0	100.9	70.9	96.6
ΣV^3 (m^3/s^3)	3579	1652	2337	2654	2920	6846	4238	2978	4058

We can assume that such a situation was observed not only in 2018, but also in 2015. In the latter, the wind impact was strongest for the entire period 2010–2018 (about 1.7 times stronger than in 2018—see Table 4), and the salinity in the 0–5-m layer was slightly higher than in 2018 (Figure 10). This was not even prevented by quite strong precipitation (total for the period about twice as much as in 2018—see Table 3). Unfortunately, in 2015, there were no direct measurements of the CDOM absorption, but the estimate from satellite data shows that, in June, the values of a_g were not lower than in 2018—see Figure 2).

Author Contributions: Conceptualization and methodology, O.K.; software, validation, investigation, and visualization, A.Y., S.V., and I.S.; writing—original draft preparation, A.Y. and O.K.

Funding: This research received no external funding.

Acknowledgments: The results were obtained in the framework of the state assignment of Minobrnauki RF (theme No. 0149-2019-0003). We are grateful to GSFC DAAC for providing the satellite data of MODIS and SeaWiFS. We thank S.I. Pogosyan for a given opportunity to use the ICAM absorption meter in our expeditionary research, A.G. Zatsepin for useful discussion and important tips, V.A. Artemiev, O.I. Podymov, V. Ocherednik, S.A. Mosharov, V.A. Silkin, and L.A. Pautova for providing data of related measurements, and S.V. Sheberstov for help with computer processing. We also thank both anonymous reviewers for their useful comments, especially reviewer 2 for detailed comments in both revisions.

Conflicts of Interest: The authors declare no conflict of interest.

References

- Burenkov, V.I.; Kelbalikhanov, B.F.; Kopelevich, O.V. Methods of measurements of the seawater optical properties. In *Ocean Optics*; Monin, A.S., Ed.; Nauka: Moscow, Russia, 1983; Volume 1, pp. 131–139.
- Kopelevich, O.V.; Rusanov, S.J.; Nosienko, N.M. Light absorption by sea water. In *Hydrophysical and Hydrooptical Investigations in the Atlantic and Pacific Oceans in View of Results of the 5th Cruise of r/v “Dimitry Mendeleev”*; Nauka: Moscow, Russia, 1974; pp. 107–112.
- Kopelevich, O.V.; Burenkov, V.I. On the relationship between spectral light attenuation coefficients of sea water, phytoplankton pigments and yellow substances. *Okeanology* **1977**, *17*, 427–433.
- Kopelevich, O.V.; Lyutsarev, S.V.; Rodionov, V.V. The spectral absorption of light by yellow substance in ocean water. *Oceanology* **1989**, *29*, 409–414.
- Kalle, K. The problem of Gelbstoff in the sea. *Oceanogr. Mar. Biol. Annu. Rev.* **1966**, *4*, 91–104.
- Højerslev, N.K. On the origin of yellow substance in the marine environment. *Oceanogr. Rep. Univ. Cph. Inst. Phys.* **1980**, *42*, 1–35.
- Bricaud, A.; Morel, A.; Prieur, L. Absorption by dissolved organic matter of the sea (yellow substance) in the UV and visible domains. *Limnol. Oceanogr.* **1981**, *26*, 43–53. [[CrossRef](#)]

8. Carder, K.L.; Steward, R.G.; Harvey, G.R.; Ortner, P.B. Marine humic and fulvic acids: Their effects on remote sensing of ocean chlorophyll. *Limnol. Oceanogr.* **1989**, *34*, 68–81. [[CrossRef](#)]
9. Wozniak, B.; Dera, J. *Light Absorption in Sea Water*; Springer: New York, NY, USA, 2007.
10. Koblentz-Mishke, O.I.; Wozniak, B.; Ochakovskiy, Y.E. *Utilisation of Solar Energy in the Photosynthesis of the Baltic and Black Sea Phytoplankton*; Izd. Inst. Okeanol.; AN SSSR: Moscow, Russia, 1985.
11. Koblentz-Mishke, O.I.; Wozniak, B.; Kaczmarek, S.; Kononov, B.V. The assimilation of light energy by marine phytoplankton. Part 1. The light absorption capacity of the Baltic and Black Sea phytoplankton (methods; relation to chlorophyll concentration). *Okeanology* **1995**, *37*, 145–169.
12. Churilova, T.; Berseneva, G. Absorption of light by phytoplankton, detritus, and dissolved organic substances in the coastal region of the Black Sea (July–August 2002). *Phys. Oceanogr.* **2004**, *14*, 221–233. [[CrossRef](#)]
13. Suslin, V.; Churilova, T. A regional algorithm for separating light absorption by chlorophyll-a and coloured detrital matter in the Black Sea, using 480–560 nm bands from ocean colour scanners. *Int. J. Remote Sens.* **2016**, *37*, 4380–4400. [[CrossRef](#)]
14. Kopelevich, O.V.; Burenkov, V.I.; Sheberstov, S.V.; Vazyulya, S.V.; Kravchishina, M.D.; Pautova, L.; Silkin, V.A.; Artemiev, V.A.; Grigoriev, V. Satellite monitoring of coccolithophore blooms in the Black Sea from ocean color data. *Remote Sens. Environ.* **2014**, *146*, 113–123. [[CrossRef](#)]
15. Kopelevich, O.V.; Burenkov, V.I.; Sheberstov, S.V. Case Studies of Optical Remote Sensing in the Barents Sea. In *Remote Sensing of the European Seas*; Springer: Dordrecht, The Netherlands, 2008; pp. 53–66.
16. Kopelevich, O.V.; Sheberstov, S.V.; Burenkov, V.I.; Vazyulya, S.V.; Pautova, L.A.; Silkin, V.A. New data about coccolithophore blooms in the Black Sea from satellite data. In Proceedings of the VII International Conference «Current problems in Optics of Natural Waters», St.-Peterburg, Russia, 10–14 September 2013; pp. 10–14.
17. Kopelevich, O.V.; Burenkov, V.I.; Sheberstov, S.V.; Vazyulya, S.V.; Sahling, I.V. Coccolithophore Blooms in the North-Eastern Black Sea. In Proceedings of the Twelfth International Conference on the Mediterranean Coastal Environment, Varna, Bulgaria, 6–10 October 2015; MEDCOAST, Mediterranean Coastal Foundation: Dalyan, Turkey, 2015; Volume 1, pp. 363–374.
18. Thierstein, H.R.; Young, J.R. *Coccolithophores—From Molecular Processes to Global Impact*; Springer: Berlin, Germany, 2004.
19. Kopelevich, O.V.; Sahling, I.V.; Vazyulya, S.V.; Glukhovets, D.I. *Bio-Optical Characteristics of the Seas, Surrounding the Western part of Russia, from Data of the Satellite Ocean Color Scanners of 1998–2017*; Burenkov, V.I., Karalli, P.G., Eds.; OOO «VASH FORMAT»: Moscow, Russia, 2018.
20. Kopelevich, O.V.; Sahling, I.V.; Vazyulya, S.V.; Glukhovets, D.I.; Sheberstov, S.V.; Burenkov, V.I.; Karalli, P.G.; Yushmanova, A.V. Atlas “Bio-Optical Characteristics of the Seas, Surrounding the Western part of Russia, from Data of the Satellite Ocean Color Scanners of 1998–2017”. Available online: <http://optics.ocean.ru/> (accessed on 30 June 2019).
21. Pogosyan, S.I.; Durgaryan, A.M.; Konyukhov, I.V.; Chivkunova, O.B.; Merzlyak, M.N. Absorption spectroscopy of microalgae, cyanobacteria, and dissolved organic matter: Measurements in an integrating sphere cavity. *Oceanology* **2009**, *49*, 866–871. [[CrossRef](#)]
22. Podymov, O.I.; Zatsepin, A.G. Seasonal anomalies of water salinity in the Gelendzhik region of the Black Sea according to shipborne monitoring data. *Oceanology* **2016**, *56*, 342–354. [[CrossRef](#)]
23. Glukhovets, D.I.; Sheberstov, S.V.; Kopelevich, O.V.; Zaytseva, A.F.; Pogosyan, S.I. Measuring the sea water absorption factor using integrating sphere. *Light Eng.* **2018**, *26*, 120–126. [[CrossRef](#)]
24. Artemiev, V.A.; Taskaev, V.R.; Burenkov, V.I.; Grigoriev, A.V. Universal compact meter of vertical distribution of light attenuation. In *Comprehensive Studies of the World Ocean: Project “Meridian”, Part 1. Atlantic Ocean*; Nauka: Moscow, Russia, 2008.
25. Dee, D.P.; Uppala, S.M.; Simmons, A.J.; Berrisford, P.; Poli, P.; Kobayashi, S.; Andrae, U.; Balmaseda, M.A.; Balsamo, G.; Bauer, P.; et al. The ERA-Interim reanalysis: Configuration and performance of the data assimilation system. *Q. J. R. Meteorol. Soc.* **2011**, *137*, 553–597. [[CrossRef](#)]
26. Emersit Data. Available online: <http://www.emercit.com/> (accessed on 30 June 2019).
27. NASA’s OceanColor Web. Available online: <https://oceancolor.gsfc.nasa.gov/> (accessed on 30 June 2019).
28. Werdell, P.J.; McKinna, L.I.W.; Boss, E.; Ackleson, S.G.; Craig, S.E.; Gregg, W.W.; Lee, Z.; Maritorena, S.; Roesler, C.S.; Rousseaux, C.S.; et al. An overview of approaches and challenges for retrieving marine inherent optical properties from ocean color remote sensing. *Prog. Oceanogr.* **2018**, *160*, 186–212. [[CrossRef](#)]

29. Sheberstov, S.V. System for batch processing of oceanographic satellite data. *Mod. Probl. Remote Sens. Earth Space* **2015**, *12*, 154–161.
30. Gordon, H.R. Can the Lambert–Beer law be applied to the diffuse attenuation coefficient of ocean water? *Limnol. Oceanogr.* **1989**, *34*, 1389–1409. [[CrossRef](#)]
31. Burenkov, V.I.; Ershova, S.V.; Kopelevich, O.V.; Sheberstov, S.V.; Shevchenko, V.P. An Estimate of the Distribution of Suspended Matter in the Barents Sea Waters on the Basis of the SeaWiFS Satellite Ocean Color Scanner. *Oceanology* **2001**, *41*, 622–628.
32. Pope, R.M.; Fry, E.S. Absorption spectrum (380–700 nm) of pure water. I. Integrating cavity measurements. *Appl. Opt.* **1997**, *36*, 8710–8723. [[CrossRef](#)] [[PubMed](#)]



© 2019 by the authors. Licensee MDPI, Basel, Switzerland. This article is an open access article distributed under the terms and conditions of the Creative Commons Attribution (CC BY) license (<http://creativecommons.org/licenses/by/4.0/>).